

## Structure-Activity Relationship of 2,4-dichloro-N-(3,5-dichloro-4-(quinolin-3-yloxy)phenyl)benzenesulfonamide (INT131) Analogs for PPAR $\alpha$ -Targeted Antidiabetics

Rebecca L Frkic, Beatriz B. Rodriguez, Mi Ra Chang, Dana Kuruvilla, Anthony Ciesla, Andrew D. Abell, Theodore M. Kamenecka, Patrick R. Griffin, and John B Bruning

*J. Med. Chem.*, **Just Accepted Manuscript** • Publication Date (Web): 09 May 2017

Downloaded from <http://pubs.acs.org> on May 10, 2017

### Just Accepted

“Just Accepted” manuscripts have been peer-reviewed and accepted for publication. They are posted online prior to technical editing, formatting for publication and author proofing. The American Chemical Society provides “Just Accepted” as a free service to the research community to expedite the dissemination of scientific material as soon as possible after acceptance. “Just Accepted” manuscripts appear in full in PDF format accompanied by an HTML abstract. “Just Accepted” manuscripts have been fully peer reviewed, but should not be considered the official version of record. They are accessible to all readers and citable by the Digital Object Identifier (DOI®). “Just Accepted” is an optional service offered to authors. Therefore, the “Just Accepted” Web site may not include all articles that will be published in the journal. After a manuscript is technically edited and formatted, it will be removed from the “Just Accepted” Web site and published as an ASAP article. Note that technical editing may introduce minor changes to the manuscript text and/or graphics which could affect content, and all legal disclaimers and ethical guidelines that apply to the journal pertain. ACS cannot be held responsible for errors or consequences arising from the use of information contained in these “Just Accepted” manuscripts.

1  
2  
3  
4  
5  
6  
7  
8  
9  
10  
11  
12  
13  
14  
15  
16  
17  
18  
19  
20  
21  
22  
23  
24  
25  
26  
27  
28  
29  
30  
31  
32  
33  
34  
35  
36  
37  
38  
39  
40  
41  
42  
43  
44  
45  
46  
47  
48  
49  
50  
51  
52  
53  
54  
55  
56  
57  
58  
59  
60

# Structure-Activity Relationship of 2,4-dichloro-N-(3,5-dichloro-4-(quinolin-3-yloxy)phenyl)benzenesulfonamide (INT131) Analogs for PPAR $\gamma$ -Targeted Antidiabetics

Rebecca L. Frkic<sup>a</sup>, Beatriz B. Rodriguez<sup>c</sup>, Mi Ra Chang<sup>b</sup>, Dana Kuruvilla<sup>b</sup> Anthony Ciesla<sup>b</sup>, Andrew D. Abell<sup>c</sup>, Theodore Kamenecka<sup>b</sup>, Patrick R. Griffin<sup>b</sup>, and John B. Bruning<sup>a,\*</sup>

<sup>a</sup>School of Biological Sciences

<sup>c</sup>Department of Chemistry

The University of Adelaide

Adelaide, South Australia, 5005, Australia

<sup>b</sup> Department of Molecular Therapeutics, The Scripps Research Institute, Scripps Florida , Jupiter, Florida 33458, United States.

\*To whom correspondence should be addressed. John B. Bruning, School of Biological Sciences, Adelaide, South Australia, Australia, Tel.: +61 (08) 8313-5218; Fax: +61 (08) 8313-4362; E-mail: [john.bruning@adelaide.edu.au](mailto:john.bruning@adelaide.edu.au)

## ABSTRACT

Peroxisome Proliferator-Activated Receptor  $\gamma$  (PPAR $\gamma$ ) is a nuclear receptor central to fatty acid and glucose homeostasis. PPAR $\gamma$  is the molecular target for type 2 diabetes mellitus (T2DM) therapeutics TZDs (thiazolidinediones), full agonists of PPAR $\gamma$  with robust antidiabetic properties, which are confounded with significant side effects. Partial agonists of PPAR $\gamma$ , such as INT131 (1), have displayed similar insulin-sensitizing efficacy as TZDs, but lack many side-

1  
2  
3 effects. To probe the structure-activity relationship (SAR) of the scaffold 1, we synthesized 14  
4  
5 analogs of compound 1 which revealed compounds with higher transcriptional potency for  
6  
7 PPAR $\gamma$  and identification of moieties of the scaffold 1 key to high transcriptional potency. The  
8  
9 sulfonamide linker is critical to activity, substitutions at position 4 of the benzene ring A were  
10  
11 associated with higher transcriptional activity, substitutions at position 2 aided in tighter  
12  
13 packing and activity, and the ring type and size of ring A affected the degree of activity.  
14  
15

## 16 17 INTRODUCTION

18  
19  
20  
21 The Peroxisome Proliferator-Activated Receptor  $\gamma$  (PPAR $\gamma$ ) is a transcription factor and member of  
22  
23 the multi-domain ligand-modulated nuclear receptor superfamily. PPAR $\gamma$  performs its function in part  
24  
25 through heterodimerization with the nuclear receptor Retinoid X Receptor  $\alpha$  (RXR $\alpha$ ) and binding to  
26  
27 DNA response elements in the proximal promoter region of target genes to regulate their expression.  
28  
29 PPAR $\gamma$  target genes include proteins involved in peripheral insulin sensitivity, adipogenesis, fatty acid  
30  
31 uptake and storage, glucose homeostasis, and metabolism of lipids and carbohydrates<sup>1-4</sup>. The array of  
32  
33 PPAR $\gamma$  target genes makes this receptor essential for normal insulin sensitivity and proper regulation  
34  
35 of blood glucose. For instance, dominant negative partial loss of function mutations in PPAR $\gamma$  cause  
36  
37 severe insulin resistance and are often accompanied by the onset of type 2 diabetes<sup>5</sup>. Adipose depots  
38  
39 secrete various cytokines and fat cell specific hormones called adipokines including adiponectin,  
40  
41 adipisin, and resistin, many of which are under direct or indirect transcriptional control of PPAR $\gamma$ <sup>6</sup>.  
42  
43 These proteins modulate insulin sensitivity of muscle, liver and adipose depots. An imbalance in this  
44  
45 process leads to the development of insulin resistance and eventually type 2 diabetes.  
46  
47

48  
49 The key role of PPAR $\gamma$  in metabolism has made it an appealing target for therapeutics of type  
50  
51 2 diabetes. The thiazolidinedione (TZD) class of PPAR $\gamma$  modulators, rosiglitazone (Avandia,  
52  
53 GlaxoSmithKline) and Pioglitazone (Actos, Takeda), bind tightly within the ligand binding pocket of  
54  
55 PPAR $\gamma$  and fully agonize the receptor by driving the interaction of the receptor with transcriptional  
56  
57 co-activator proteins. Although TZDs afford robust insulin sensitization and normalization of blood  
58  
59  
60

1  
2  
3 glucose in T2DM patients, treatment with TZDs has been linked to an array of adverse side effects  
4 which has significantly reduced their utility. TZD side effects include weight gain, increased  
5 adipogenesis, renal fluid retention, loss of bone density, congestive heart failure, and plasma volume  
6 expansion leading to hemodilution<sup>1, 7, 8</sup>. The exact causes of edema and myocardial infarction  
7 exhibited by some patients using TZD antidiabetics have not yet been elucidated to date. Given that  
8 PPAR $\gamma$  is a promiscuous binder of low affinity fatty acids and other metabolic signaling molecules,  
9 one possibility is that side effects arise from disruption of the natural signaling processes by a very  
10 high affinity agonist such as rosiglitazone, hyperactivation of target genes yet unidentified, or off-  
11 target interactions. However, ligands of PPAR $\gamma$  that only partially agonize the receptor have been  
12 shown to have reduced side-effect profiles in preclinical species and in some cases in clinical trials,  
13 yet they maintain robust insulin-sensitizing properties<sup>9, 10</sup>. These observations suggest that insulin  
14 sensitization can be separated from some if not all of the adverse effects associated with TZDs.  
15 Previous structural analysis of partial agonists of PPAR $\gamma$  demonstrated that their unique  
16 transcriptional output is attributed to distinct binding mechanisms<sup>1, 11</sup>, suggesting that structural  
17 properties of PPAR $\gamma$  ligands can govern their therapeutic index as T2DM therapeutics.

18  
19  
20  
21  
22  
23  
24  
25  
26  
27  
28  
29  
30  
31  
32  
33  
34 The PPAR $\gamma$  compound 2,4-dichloro-N-(3,5-dichloro-4-(quinolin-3-  
35 yloxy)phenyl)benzenesulfonamide **1** (INT131) is a highly potent ligand of PPAR $\gamma$ , with a  $K_i$  of 10nM  
36 in ligand-displacement direct binding assays, sufficient to displace rosiglitazone from the ligand  
37 binding pocket<sup>11</sup>. **1** is highly potent in cell based transcriptional activation assays, with an  $EC_{50}$  value  
38 of 4nM and a maximal transcriptional activation of reporter genes of approximately 30% as compared  
39 to rosiglitazone. Distinct coregulatory recruitment profiles of **1**, as compared to full agonists such as  
40 rosiglitazone, have been shown through cell based functional assays<sup>11</sup>. *In vivo* studies in rodents  
41 have shown that **1** lowers blood glucose levels by over 30% with only a 0.3mg/kg dose compared to  
42 the 3mg/kg dose required for a similar effect using rosiglitazone. Significantly, **1** showed less total  
43 weight gain, heart weight gain, and lung weight gain than that observed with rosiglitazone  
44 administration, supporting the idea that **1** leads to less adipogenesis and fluid retention/edema.  
45 Adipocyte differentiation was not enhanced in cultured cells treated with **1** in contrast to significant  
46  
47  
48  
49  
50  
51  
52  
53  
54  
55  
56  
57  
58  
59  
60

1  
2  
3 induction with rosiglitazone treatment. Phase 1 studies with **1** (4 studies) showed favorable  
4 pharmacokinetic and pharmacodynamic properties<sup>4</sup>. Phase 2a studies have demonstrated through a  
5 multicenter, double blind, placebo controlled study with T2DM patients that **1** is generally well  
6 tolerated while displaying antidiabetic effects<sup>12, 13</sup>; however, there are no publications available  
7 related to phase 2b or phase 3 studies of this compound.  
8  
9

10  
11  
12 While partial agonists such as **1** have shown great promise as insulin sensitizers, their  
13 mechanism of action has been less forth-coming. Antidiabetic effects have been shown to be  
14 correlated to blocking of phosphorylation of the receptor at position Ser273 of the ligand binding  
15 domain (LBD) by CDK5-activated ERK. Blockage of pS273 normalizes PPAR $\gamma$  target genes that are  
16 repressed in the diabetic and obese state<sup>7, 14</sup>. However, the structural mechanism of this phenomenon  
17 is not well understood.  
18  
19

20  
21  
22 PPAR $\gamma$  is a multi-domain protein containing a highly conserved DNA binding domain and a  
23 structurally conserved LBD. The LBD of PPAR $\gamma$  is comprised of 13  $\alpha$ -helices (H1-H12 and H2') and  
24 a small  $\beta$ -sheet. The binding pocket within the LBD is large enough (approximately 1200  $\text{\AA}^3$ ) to  
25 accommodate binding of a wide range of structurally distinct ligands, and the exact nature of the  
26 endogenous ligand remains controversial<sup>15</sup>. Within the LBD is the AF2 surface which is formed by  
27 helices 3-5 and helix 12, and is important for ligand-dependent cofactor binding<sup>1, 2, 16</sup>. The TZD head  
28 group of full agonists such as rosiglitazone have been shown to stabilize helix 12 and the AF2 by  
29 means of a tight hydrogen bond network allowing for co-activator binding, as well as making  
30 hydrophobic contacts with H3 and stabilizing hydrogen bonding with the beta-sheet. Interestingly,  
31 partial agonists of the receptor have been shown to require no stabilization of helix 12 for  
32 transcriptional activation<sup>1</sup>.  
33  
34  
35  
36  
37  
38  
39  
40  
41  
42  
43  
44  
45  
46  
47

48 In order to better define the specific chemical epitopes of **1** responsible for high  
49 transcriptional activity, we developed a SAR platform correlating chemistry, potency based on  
50 activity, and protein structure. Here we present fourteen analogs of **1**. These analogs were tested for  
51 their ability to transcribe target genes (potency) in a cellular reporter assay allowing us to compare  
52 activity to structure by means of EC<sub>50</sub> values. An X-ray crystal structure was obtained for one of the  
53  
54  
55  
56  
57  
58  
59  
60

1  
2  
3 analogs, 4-bromo-N-(3,5-dichloro-4-(quinolin-3-yloxy)phenyl)-2,5-difluorobenzenesulfonamide (**10**),  
4  
5 bound to the PPAR $\gamma$  ligand binding domain to a resolution of 2.2Å. The binding mode of the other 13  
6  
7 analogs was deciphered by means of *in silico* docking methods. The analogs displayed a wide range  
8  
9 of activity from an EC<sub>50</sub> of 2nM to no binding at all, allowing us to define several important moieties  
10  
11 in the structure-activity of the compound **1** scaffold. These analogs allowed us to define the  
12  
13 sulphonamide linker, positions 2 and 4 of benzene ring A, as well as the nature and position of the  
14  
15 substituents in ring A as being most important for defining high potency.  
16  
17  
18  
19

## 20 RESULTS & DISCUSSION

21  
22  
23  
24 **Design and activity of compound 1 analogs.** Compound **1** is a 514 Da sulfonamide  
25  
26 compound comprised of three major aromatic moieties, denoted A, B, and C (Figure 1). A is a 2,4 di-  
27  
28 Cl benzene linked by a sulphonamide to a 3, 5 di-Cl aniline moiety (with aniline nitrogen as atom 1)  
29  
30 denoted B. Ring system C is a quinoline moiety joined to B by an ether linker. The co-crystal  
31  
32 structure of **1** bound to PPAR $\gamma$  has been solved <sup>11</sup>, which shows that, unlike TZDs, **1** does not contact  
33  
34 and stabilize helix 12 but instead wraps around helix 3 to stabilize helix 3 and the  $\beta$ -sheet region <sup>11</sup>  
35  
36 (Figure 2). The ligand forms two hydrogen bonds with Tyr327 of helix 5, which donates a hydrogen  
37  
38 to the S=O group of **1** and accepts a hydrogen from the sulfonamide N-H in the center of the  
39  
40 compound. A displaced parallel *pi-pi* interaction between the head group ring (ring A) of **1** and  
41  
42 Phe363 of helix 7 situated 3.7Å away further promotes ligand binding. The apolar region generated by  
43  
44 Ile341, Cys285, Gly284, and Phe363 is also important for its interaction with the aromatic rings of **1**.  
45  
46

47  
48 Previous structure-activity data has indicated that the composition of the C ring system of **1**  
49  
50 had profound effects on CYP450 inhibition (CYP3A4). Specifically, the presence of a pyridine ring  
51  
52 in the C position of **1** led to potent CYP3A4 inhibition (IC<sub>50</sub> 1nM $\rightarrow$ 1 $\mu$ M) <sup>4</sup>. However, changing the C  
53  
54 ring from pyridine to quinoline showed the highest affinity PPAR $\gamma$  direct binding with significantly  
55  
56 reduced CYP3A4 inhibition. Additionally, Cl substitution of positions R5 and R6 of the B ring aniline  
57  
58 demonstrated the highest affinity PPAR $\gamma$  direct binding and transactivation <sup>4</sup>. In order to define the  
59  
60

1  
2  
3 structure activity relationship of compound **1** analogs, we focused on altering the substitution of the A  
4 ring given the need for a quinoline group in the C ring for drug metabolism reasons and the need for a  
5 dichloro-aniline ring at the B position for affinity reasons. The purpose of our SAR is to precisely  
6 define what chemical epitopes of **1** and, conversely, what regions of the PPAR $\gamma$  LBD need to be  
7 stabilized for optimum affinity as well as transactivation. Additionally, given the appeal of  
8 antagonists of PPAR $\gamma$  as therapeutic agents, compound **1** analogs with reduced transactivation  
9 potential are likely to be required for an attractive therapeutic profile with a very low or no incidence  
10 of side effects.  
11  
12  
13  
14  
15  
16  
17  
18  
19

20  
21 14 analogs of **1** (as well as **1**) were synthesized with various alterations of the A ring (Table  
22 1) including one previously reported compound, (4-bromo-N-(3,5-dichloro-4-(quinolin-3-  
23 yloxy)phenyl)-2-(trifluoromethoxy)benzenesulfonamide, described in our assays as compound **3**<sup>4</sup>.  
24 Synthesis was performed following reported protocols as in the materials and methods <sup>4</sup>.  
25 Substitutions of the benzene ring included Br, F, CF<sub>3</sub>, O-CH<sub>3</sub>, as well as CH<sub>3</sub> at varying positions.  
26 The benzene ring was substituted for rings of a different nature in two of the compounds: a  
27 naphthalene ring system (N-(3,5-dichloro-4-(quinolin-3-yloxy)phenyl)naphthalene-2-sulfonamide  
28 (**12**) and a thiophene ring N-(3,5-dichloro-4-(quinolin-3-yloxy)phenyl)thiophene-2-sulfonamide (**15**).  
29 These substituents were chosen to probe the effect of having a ring other than benzene in the A ring  
30 position of **1**. All compounds contained a sulfonamide linker to the A ring with the exception of N-  
31 (3,5-dichloro-4-(quinolin-3-yloxy)phenyl)thiophene-2-carboxamide (**7**) containing an amide linker to  
32 the A ring in order to probe the effect on binding and activity of substitution at this position.  
33  
34  
35  
36  
37  
38  
39  
40  
41  
42  
43  
44

45 All compounds were tested for activity against PPAR $\gamma$  in a cell based transcriptional reporter  
46 assay to measure both potency (EC<sub>50</sub>) as well as the maximal transcriptional output as normalized to  
47 the model full agonist rosiglitazone (transactivation = 100%). Potencies of the compounds ranged  
48 from 2nM (**3**) to no activity (**7**). All EC<sub>50</sub> and maximal transactivation values can be found in Table 1  
49 for all compounds. The maximum transactivation level for **1** was 24% and our analogs displayed  
50 maximum transactivation levels in the range of 2-34%, indicating that all compounds were partial  
51 agonists.  
52  
53  
54  
55  
56  
57  
58  
59  
60

1  
2  
3  
4  
5 **Structural analysis of compound 1 analogs in complex with PPAR $\gamma$ .** In order to probe the  
6 structural basis of **1** analog potency, we performed co-crystallization experiments of compound **1**  
7 analogs with PPAR $\gamma$ . Co-crystals were only obtained for 4-bromo-N-(3,5-dichloro-4-(quinolin-3-  
8 yloxy)phenyl)-2,5-difluorobenzenesulfonamide (**10**) in complex with the PPAR $\gamma$  LBD. The PPAR $\gamma$   
9 LBD bound to **10** was solved to a resolution of 2.2Å and the phase problem was overcome by  
10 molecular replacement. Data processing and refinement statistics can be found in Table 2. The  
11 asymmetric unit contained two subunits of PPAR $\gamma$  (homodimer), conforming to the canonical PPAR $\gamma$   
12 LBD fold. The **10** bound LBD structure revealed high global similarity to previously solved  
13 structures with a 0.84Å RMSD with the LBD from the full agonist rosiglitazone bound structure (over  
14 256 C $\alpha$  atoms, PDB:2PRG), a 0.69Å RMSD with the LBD from the apo structure (over 258 C $\alpha$   
15 atoms, PDB:1PRG), and a 0.88Å RMSD with the partial agonist **1** bound LBD (over 254 C $\alpha$  atoms,  
16 PDB:3FUR)<sup>11, 17</sup>. A ribbons diagram of the **10** bound LBD can be seen in Figure 2A. The **10** ligand  
17 was easily visible in the electron density and modelled into the difference Fourier electron density. A  
18 reduced model bias electron density map of **10** can be viewed in Figure S1.

19  
20  
21  
22  
23  
24  
25  
26  
27  
28  
29  
30  
31  
32  
33  
34  
35  
36  
37  
38  
39  
40  
41  
42  
43  
44  
45  
46  
47  
48  
49  
50  
51  
52  
53  
54  
55  
56  
57  
58  
59  
60  
Compound **10** occupies the ligand binding pocket of PPAR $\gamma$  and is centered at and bends  
around helix 3; the scaffold location of **10** is similar to **1** (Figure 2B and 2C). Several weak  
electrostatic interactions are formed between the sulfonamide linker of **10** and residues of or near the  
AF2. One oxygen atom of the sulfonamide moiety of **10** is in weak hydrogen bonding distance to  
Tyr327 side chain oxygen atom (3.5Å), Lys367 side chain nitrogen atom (2.9Å), and His449 side  
chain nitrogen atom (3.5Å). This leaves Tyr473 of the AF2 helix 12 unstabilized and not within  
hydrogen bonding distance to His449 (4.6Å) as seen in full agonist bound structures. Tyr327 accepts a  
hydrogen atom from the sulfonamide N-H in the center of the **10** compound to form a 3.2Å hydrogen  
bond analogous to **1** (2.8Å). A comparable set of *pi-pi* interactions between the A ring of **10** and  
Phe363 exists and likely contributes to ligand binding affinity. **10** engages in hydrophobic contacts  
with Ile341 (beta sheet), Cys285 (H3), and Gly284 (H3), similarly to **1** (Figure 2C). **10** contains a Br

1  
2  
3 atom at position 4 of the A ring (in contrast to a Cl in **1**) which is in weak halogen bonding distance to  
4  
5 the main chain nitrogen atom of Phe282 (3.7Å).  
6

7 *In silico* docking of all other ligands (those other than **10**) shown to bind to the PPAR $\gamma$  LBD  
8  
9 was carried out using a Monte Carlo method in the Molsoft ICM Software suite to identify the binding  
10  
11 mechanisms of these compounds. As a positive control, **1** was docked into the PPAR $\gamma$  LBD and  
12  
13 compared to the experimentally derived X-ray crystal structure. The binding mode of the two  
14  
15 structures was nearly identical and a superimposition of the two molecules is located in Figure S2.  
16  
17 Docking of the **1** analogs revealed a similar overall binding mode for them all, with the C and B rings  
18  
19 exhibiting very high positional similarity with only minor differences in the A rings due to  
20  
21 substitution. A superimposition of the ligands docked to the receptor can be found in Figure 3.  
22  
23

24  
25 **The sulfonamide moiety is essential for binding to PPAR $\gamma$ .** The A ring of **1** is located in the  
26  
27 hydrophobic pocket between H3 and H7, making not only hydrophobic interactions with Cys285 of  
28  
29 H3 but more importantly several critical *pi-pi* interactions with Phe363. The A ring of **1** is connected  
30  
31 to the **1** scaffold via the S atom of the sulfonamide linker. The sulfur atom displays tetrahedral  
32  
33 geometry which places the connected A ring in ideal position to interact with Phe363 in a stacking  
34  
35 manner (Figure 2B).  
36

37  
38 To probe if the sulfonamide linker of **1** is necessary for activity we synthesized **7**. Table 1  
39  
40 shows that **7** shows no significant transactivation activity and contains an amide linker instead of the  
41  
42 sulfonamide of the other ligands. This substitution makes the atom which connects the A ring to the  
43  
44 compound **7** scaffold, C of the C=O, in a planar Sp<sup>2</sup> hybridized state. As shown in Figure 4, this  
45  
46 places the A ring in a location closer to the AF2 surface and incapable of making the favorable *pi-pi*  
47  
48 interactions with Phe363 as well as the favorable hydrophobic interactions in the surrounding pocket.  
49  
50 The sulfonamide moiety absent in **7** also means that there is no atom in appropriate distance to act as a  
51  
52 hydrogen bond donor or acceptor with the side chain of Tyr327. Taken together, our data thus  
53  
54 suggests that the A ring linker geometry, and to a lesser degree interaction with Tyr327, is essential  
55  
56 for significant receptor binding and activity. This is critical for potential drug design, as the inclusion  
57  
58 of a sulfonamide moiety will substantially promote compound binding to PPAR $\gamma$ .  
59  
60

1  
2  
3  
4  
5 **Higher affinity is achieved with Br at position 4 of benzene ring A.** Ligands with the nine highest  
6 potencies (2-957nM) all have a Br atom at position 4 of the A ring (4-bromo-N-(3,5-dichloro-4-  
7 (quinolin-3-yloxy)phenyl)-3-methylbenzenesulfonamide (**2**), **3**, 4-bromo-2-chloro-N-(3,5-dichloro-4-  
8 (quinolin-3-yloxy)phenyl)benzenesulfonamide (**4**), 4-bromo-N-(3,5-dichloro-4-(quinolin-3-  
9 yloxy)phenyl)-3-(trifluoromethyl)benzenesulfonamide (**5**), 4-bromo-N-(3,5-dichloro-4-(quinolin-3-  
10 yloxy)phenyl)-2-(trifluoromethyl)benzenesulfonamide (**6**), 4-bromo-N-(3,5-dichloro-4-(quinolin-3-  
11 yloxy)phenyl)-2-fluorobenzenesulfonamide (**8**), 4-bromo-N-(3,5-dichloro-4-(quinolin-3-  
12 yloxy)phenyl)-3-fluorobenzenesulfonamide (**9**), **10**, and 4-bromo-N-(3,5-dichloro-4-(quinolin-3-  
13 yloxy)phenyl)benzenesulfonamide (**11**). In addition, the five lowest affinity ligands (3314nM-no  
14 significant activity) all lack Br at his position. Superimposition of Br-containing compound **1** analogs  
15 at different positions in the A ring can be seen in Figure 5. Structural analysis reveals that the Br  
16 atom is located in nearly identical positions in all of these structures. This places the Br atom within  
17 distance to form a halogen bond with the back bone nitrogen atom of Phe282 (Figure 5) and allows  
18 for better packing within the ligand binding pocket through Van der Waals interactions. The halogen  
19 bond is indeed weak (4Å) and improved activity from substitution at this site with Br is perhaps  
20 associated with tighter packing of the pocket in this region. This is clearly an important observation  
21 for ongoing drug design efforts with **1** which would therefore ideally incorporate Br at this position or  
22 place a hydrogen bonding partner extending from position 4 of the A ring in proximity to the back  
23 bone nitrogen atom of Phe282.

24  
25  
26  
27  
28  
29  
30  
31  
32  
33  
34  
35  
36  
37  
38  
39  
40  
41  
42  
43  
44  
45  
46 **Tight packing within the ligand binding pocket is associated with higher activity.** Examination of  
47 space filling representations of the compound **1** analogs within the ligand binding pocket of PPAR $\gamma$   
48 shows that the highest affinity ligands are distinguished from lower affinity ligands by means of  
49 tighter molecular packing. The five ligands (**3**, **4**, **6**, **8** and **10**) with the highest affinities (2-957nM)  
50 present a substituent at position 2 on benzene ring A. These substituents contribute steric bulk to the  
51 ligand and more tightly occupies the space of the binding pocket between helices 3 and 7, increasing  
52 the strength and number of van der Waals interactions. Substitutions at position 2 of the benzene ring  
53  
54  
55  
56  
57  
58  
59  
60

1  
2  
3 A of these compounds include -F, -CF<sub>3</sub>, -Cl, and -OCF<sub>3</sub>. Van der Waals volumes for these groups  
4  
5 range from 13Å<sup>3</sup> to 100Å<sup>3</sup>, with a general trend of the smaller van der Waals volume substitutions  
6  
7 correlating with the lower activity. As shown in Figure 6A, position 2 of the benzene ring A is most  
8  
9 amenable to substitution for improved packing such that compounds with substitutions on other  
10  
11 positions do not pack as favorably in the binding pocket (Figure 6B) and induce lower activation rates  
12  
13 of the receptor. Despite **3** and **6** having very similar structures (- OCF<sub>3</sub> versus - CF<sub>3</sub>), **3** is  
14  
15 significantly more potent than **6** because the addition of the oxygen enables the trifluoro group to pack  
16  
17 deeper in the binding pocket between helices 3, 7 and 11 (Figure 6C). Furthermore, this extension also  
18  
19 enables two of the fluorine atoms to be within halide bond distance (both approximately 3Å) of the  
20  
21 side chain nitrogen atom of Gln286, which further increases the compound's affinity for PPAR $\gamma$ .  
22  
23

24  
25 **Divergence from aromatic benzene ring A does not favor high activity.** Two of the compound **1**  
26  
27 analogs (**12** and **15**) differ from the otherwise conserved A-ring containing a single aromatic benzene.  
28  
29 These two ligands have very low potencies (4289nM and ND respectively). This suggests that the six-  
30  
31 membered aromatic ring is optimal for PPAR $\gamma$  activity. **12** has a naphthalene moiety, sizably  
32  
33 enhancing its hydrophobicity at this position as compared to the other analogs (Figure 7). Despite  
34  
35 having many more interactions with hydrophobic residues of the binding pocket, its potency is poor,  
36  
37 with an EC<sub>50</sub> of 4289nM. This may be due to the nature of the aromatic system. Rings B and C of **12**  
38  
39 are in nearly identical positions to the B and C rings of **1** and other analogs (Figure 3), suggesting that  
40  
41 differences in activity lie solely in the A ring. Additionally, the naphthalene moiety of **12** is in a  
42  
43 parallel displaced stacking interaction with Phe363 positioned similarly to ring A of the other analogs.  
44  
45 While the naphthalene group is larger than the benzene ring A of the other analogs, it packs well  
46  
47 without clashing into the hydrophobic pocket of the LBD between H3 and H7 (Figure 6D). Although  
48  
49 **12** can form stacking interactions with Phe363, the activity is much lower than the other compound **1**  
50  
51 analogs implying that differences in affinity may lie in the absence of substitutions on the naphthalene  
52  
53 group. **12** is the only compound that lacks a substituent on the A ring. The Hunter/Sanders model has  
54  
55 demonstrated that electron withdrawing substituents, such as the halides, diminish electron density in  
56  
57 the *pi* cloud of the ring leading to enhanced *pi*-stacking<sup>18</sup>. This is consistent with our data in which  
58  
59  
60

1  
2  
3 the electron withdrawing substitutions of the A ring such as F, Br, and Cl show stronger activity. In  
4 agreement with this hypothesis, is compound N-(3,5-dichloro-4-(quinolin-3-yloxy)phenyl)-2,4,6-  
5 trimethylbenzenesulfonamide (**14**) which is substituted with no electron withdrawing groups, only  
6 methyl groups (electron donating), which also shows diminished activity as compared to the analogs  
7 with electron withdrawing substitutions.  
8  
9

10  
11  
12  
13 Compound **15**, where the benzene ring was replaced by a thiophene moiety, showed no data  
14 in terms of potency for the receptor. Importantly, **15** does not make *pi-pi* interactions with Phe363,  
15 with the component thiophene known to be less aromatic than benzene, which provides less  
16 availability for *pi-pi* interaction, likely decreasing binding affinity. It could be postulated that the  
17 interaction with Phe363 favors higher affinity ligands. Critically, structural analysis also demonstrated  
18 **15** does not pack as well in the PPAR $\gamma$  LBD due to the lack of substitution patterns characteristic of  
19 the higher-affinity compounds. This includes a halide at position 4, and steric bulk in positions 2 or 3.  
20 The five-membered thiophene ring does not pack as tightly in the hydrophobic pocket as the other  
21 analogs due to lack of substitution as well as the smaller, five-membered ring size. This, taken  
22 together, suggests that a single aromatic benzene forms the best scaffold for ring A.  
23  
24  
25  
26  
27  
28  
29  
30  
31  
32

### 33 34 35 **Substitutions at benzene ring A of compound 1 have modest effects on the degree of agonism.**

36  
37 Given the promise of PPAR antagonists as a novel class of antidiabetics with little or no side effects,  
38 decreasing the degree of agonism of **1** would be ideal. There is some variation in the level of  
39 transactivation of the receptor among all of the compound **1** analogs we surveyed as maximum  
40 transactivation rates were in the range of 2-34%. While this is a similar transactivation rate from the  
41 compound **1** parent compound (24% maximal transactivation) further decreases in transactivation will  
42 require more SAR efforts. Our data suggests that modifying the ligands at the A ring moiety affects  
43 only their affinities for the receptor, and not their level of agonism. Comparing the binding  
44 mechanisms of the current compounds with full agonists demonstrates that they bind in different  
45 positions and this governs their level of transcriptional output. The consistent binding mechanisms of  
46 the partial agonists can be attributed to the presence of the conserved regions of rings B and C. It is  
47 important for design of T2DM therapeutics using the compound **1** scaffold to include these moieties,  
48  
49  
50  
51  
52  
53  
54  
55  
56  
57  
58  
59  
60

1  
2  
3 so that the compound will have high affinity binding while not fully agonizing the receptor. Lessons  
4 from other scaffolds have revealed that reducing agonism can be achieved through destabilization of  
5 the AF2 surface and H12. Hence, future compound **1** based therapeutics with lessened transcriptional  
6 activation may be achieved through substitution of the quinolone ring extending to H12 to form  
7 destabilizing contacts.  
8  
9  
10  
11  
12

## 13 14 15 **CONCLUSION**

16  
17  
18  
19 We have described here the synthesis of 14 analogs of the antidiabetic compound **1** by means of  
20 chemical alteration of the A ring. This study includes protein structural studies which when combined  
21 with transcriptional activation assays (which measure potency of the compound **1** analogs) allow the  
22 derivation of precise structure-activity relationships of these compounds. This SAR study defined the  
23 effects that substituents of the A ring, position of substituents on the A ring, and the type of ring at  
24 position A have on transcriptional activity and, more importantly, how these substituents affect  
25 interaction of the compound **1** scaffold with the PPAR $\gamma$  receptor. SAR of compound **1** analogs  
26 revealed seven ligands with increased potency for PPAR $\gamma$ . These maintained the sulfonamide moiety  
27 and a bromine atom at position 4 on the aromatic benzene ring A. They differ from **1** in their  
28 substitutions which enable better lock-and-key fitting in the binding pocket of PPAR $\gamma$ , mediated by  
29 the presence of a bulky substitution at position 2 of benzene A. Additionally, the SAR data  
30 demonstrates the importance of a sulfonamide linker as well as a substituted, 6-membered benzyl ring  
31 in position A. Taken together, these results present a clearer picture of the molecular mechanism of **1**  
32 and how future drug discovery efforts for new therapeutics targeting PPAR $\gamma$  can be tailored for higher  
33 potency.  
34  
35  
36  
37  
38  
39  
40  
41  
42  
43  
44  
45  
46  
47  
48  
49  
50  
51  
52  
53

## 54 **EXPERIMENTAL SECTION**

55  
56  
57  
58  
59  
60

1  
2  
3 **Transactivation assay.** 4.5  $\mu\text{g}$  human GAL4-PPAR $\gamma$ -Hinge-LBD, 4.5  $\mu\text{g}$  5x multimerized UAS-  
4 luciferase reporter, and 27 $\mu\text{L}$  X-treme Gene 9 transfection reagent were cotransfected into HEK293T  
5 cells (ATCC; cat. no. CRL-3216) and grown in serum-free Opti-MEM reduced serum media (Gibco).  
6  
7 The Gal4-pBind vector and UAS-LUC were co-transfected into cells as a control. Cells were grown  
8  
9 for 18h at 37°C in a 5% CO<sub>2</sub> incubator after which they were plated in quadruplicate in white 384-  
10 well plates (PerkinElmer) at a density of 10,000 cells in each well. Cells were treated with either  
11  
12 DMSO only or the compound of interest (doses from 169pM to 10 $\mu\text{M}$ ) after replating. Cells were  
13  
14 treated with Brite Lite Plus (PerkinElmer) after 18 h incubation and read in a 384-well Luminescence  
15  
16 PerkinElmer EnVision Multilabel plate reader. Fold change of treated cells over DMSO-treated  
17  
18 control cells were plotted to define EC<sub>50</sub> values. GraphPad Prism was used for plotting and statistical  
19  
20 analysis including error bars. Each data point in the EC<sub>50</sub> does response was repeated in triplicate and  
21  
22 standard Error of mean (S.E.M.) was derived from these values. In addition, two biological replicates  
23  
24 were performed to ensure reproducibility of the data  
25  
26  
27  
28  
29

30 **Protein purification.** The PPAR $\gamma$  ligand binding domain (residues 205-477) including an N-terminal  
31  
32 hexa-histidine tag were encoded in the pET11 expression vector. The expression vector was  
33  
34 transformed into *E. coli* BL21(DE3). Cells were grown at 37°C in LB media containing 50 $\mu\text{g}/\text{mL}$   
35  
36 ampicillin until an optical density of 0.5 was reached. Cells were induced at 16°C for 18 hours,  
37  
38 harvested by centrifugation, resuspended in buffer A (20mM Tris 8.0, 0.5M NaCl, 10mM imidazole,  
39  
40 and 2mM BME), and stored at -80°C. Cells were lysed by three passes through a French Press. Cell  
41  
42 lysate was clarified by centrifugation at 10,000g for 1 h and applied to a 5mL His-Trap FF crude  
43  
44 column (GE Healthcare), washed with 100mL buffer A, and eluted with 25mL buffer B (20mM Tris  
45  
46 8.0, 0.5M NaCl, 250mM imidazole, and 2mM BME). The elution fractions were pooled and dialyzed  
47  
48 to buffer C (20mM Tris 8.0, 10mM NaCl, and 1mM DTT) using a 10,000 molecular weight cut-off  
49  
50 dialysis bag (Spectrum Laboratories, Inc.) for 18 hours). The PPAR $\gamma$  sample was applied to a HiPrep  
51  
52 26/60 Sephacryl S-300 HR size-exclusion column and eluted at 1mL/minute over one column  
53  
54 volume. Fractions containing purified PPAR $\gamma$  were concentrated to 10mg/mL using a 10,000  
55  
56  
57  
58  
59  
60

1  
2  
3 molecular weight cut-off centripetal concentrator (Millipore). Protein used in crystallization trials  
4  
5 was used fresh and without freeze/thaw (within three days of preparation).  
6  
7

8  
9 **Crystallization/Data Processing.** Crystallization trials were carried out with all compounds,  
10  
11 but only compound **10** produced diffracting co-crystals. For complex formation, a sample of  
12  
13 10mg/mL PPAR $\gamma$  LBD was mixed with **10** (5mM final concentration **10**) and incubated on ice for 30  
14  
15 minutes. Prior to crystallization the sample was clarified by centrifugation at 10,000 g at 4°C for 10  
16  
17 minutes and the supernatant was extracted for use in crystallization trials. Crystals were formed using  
18  
19 the vapor diffusion method by mixing 1 $\mu$ L of PPAR $\gamma$ -**10** complex with 1 $\mu$ L well solution in an Intelli-  
20  
21 plate (Art Robbins) using a sitting drop style plate. The well solution consisted of 75 $\mu$ L 2M  
22  
23 ammonium sulfate. Crystallization trials were conducted at 289 K. Cubic crystals of approximately  
24  
25 150 microns in each dimension appeared after three days. The well solution containing 15% ethylene  
26  
27 glycol was used as a cryo-protectant. Crystals were harvested using a cryo-loop (Hampton Research)  
28  
29 and flash cooled to 100 K. All data was collected at 100 K. Data was collected at APS beamline 22-  
30  
31 ID. 450 images were collected at 0.5° oscillations (225° data total) at 0.6 second exposure time per  
32  
33 image. Data was processed using iMosflm<sup>19</sup> and scaled in aimless<sup>20</sup> to a resolution of 2.2Å.  
34  
35 Resolution cut-off was determined by use of the CC1/2 criteria<sup>21</sup>. PDB:3FUR stripped of ligands and  
36  
37 water molecules was used as a search model and phases were obtained by molecular replacement in  
38  
39 Phaser<sup>22</sup>. Initial difference Fourier maps revealed clear electron density for **10** and was modelled  
40  
41 manually. Refinement, including TLS refinement, was carried out in Phenix<sup>23</sup> with multiple rounds of  
42  
43 manual rebuilding carried out in Coot<sup>24</sup>. Refinement was completed when R-factors converged.  
44  
45 Unsuccessful soaks of PPAR $\gamma$  apo crystals were diffracted at the Australian Synchrotron beamline  
46  
47 MX1 and MX2<sup>25</sup>.  
48  
49

50  
51  
52 **Docking.** The ICM Molsoft suite<sup>26</sup> was used to dock compound **1** analogs into the PPAR $\gamma$  LBD  
53  
54 structure. PDB 3FUR with ligands removed was used as the starting model for docking. The PPAR $\gamma$   
55  
56 LBD structure was prepared for docking by protonation, deletion of water molecules, and energy  
57  
58  
59  
60

1  
2  
3 minimization by means of the ICM force field and distance dependent dielectric potential with an  
4 RMS gradient of 0.1. PocketFinder within ICM was used to define the ligand binding pocket and was  
5 consistent with previously published X-ray structures. Default settings within the ICM docking  
6 module were used with a rectangular box centered at the LBD with a grid spacing of 0.5Å. The top  
7 ranked docking for each ligand was chosen for interpretation as the conformations were very  
8 consistent with scaffold placement of **1** and **10** in the X-ray crystal structure.  
9  
10  
11  
12  
13  
14  
15  
16

### 17 ASSOCIATED CONTENT

18 Additional figures (S1 and S2) illustrating sample electron density and comparison of the docking to  
19 structures derived from experimental X-ray. Details of compounds synthesis including H<sup>1</sup> NMR, MS  
20 and HPLC analysis. This material is available free of charge via the Internet at <http://pubs.acs.org>.  
21  
22  
23  
24  
25  
26

### 27 AUTHOR INFORMATION

#### 28 Corresponding Author

29 \*Phone: +61 (08) 8313 5218. E-mail: [john.bruning@adelaide.edu.au](mailto:john.bruning@adelaide.edu.au).  
30  
31  
32

#### 33 Notes

34 The authors declare no competing financial interest.  
35  
36  
37  
38  
39  
40  
41

### 42 ACKNOWLEDGEMENTS

43  
44  
45 We would like to thank the staff at SER-CAT beamline for assistance with data collection. Use of the  
46 Advanced Photon Source was supported by the U. S. Department of Energy, Office of Science, Office  
47 of Basic Energy Sciences, under Contract No. W-31-109-Eng-38. We would like to thank the staff at  
48 beamlines MX1 and MX2 of the Australian Synchrotron for help with data collection of the PPAR  
49 soaks (This work was supported by CAP6919 and CAP8221 of the AS). This work was funded in  
50 part by NIH NIDDK DK105825 PI: Griffin.  
51  
52  
53  
54  
55  
56  
57  
58  
59  
60

1  
2  
3  
4  
5 The PDB code for PPAR $\gamma$  in complex with **10** is 5TTO. Authors will release the atomic coordinates  
6  
7 and the experimental data upon article publication.  
8  
9

## 10 11 **ANCILLARY INFORMATION**

12  
13 **Molecular Formula Strings.** Strings are available in the supporting information.

14  
15 **Abbreviations.** PPAR: peroxisome proliferator activated receptor; TZD: thiazolidinedione;  
16  
17 SAR: structure activity relationship; RXR: retinoid X receptor; T2DM: Type II Diabetes  
18  
19 Mellitus.  
20  
21

## 22 23 **REFERENCES**

- 24  
25  
26  
27  
28 (1) Bruning, J. B.; Chalmers, M. J.; Prasad, S.; Busby, S. A.; Kamenecka, T. M.; He, Y.; Nettles,  
29  
30 K. W.; Griffin, P. R. Partial agonists activate PPAR $\gamma$  using a helix 12 independent mechanism.  
31  
32 *Structure* **2007**, *15*, 1258-1271.
- 33  
34 (2) Kroker, A. J.; Bruning, J. B. Review of the structural and dynamic mechanisms of  
35  
36 PPAR $\gamma$  partial agonism. *PPAR Res.* **2015**, *2015*: 816856.
- 37  
38 (3) van Marrewijk, L. M.; Polyak, S. W.; Hijnen, M.; Kuruvilla, D.; Chang, M. R.; Shin, Y.;  
39  
40 Kamenecka, T. M.; Griffin, P. R.; Bruning, J. B. SR2067 Reveals a unique kinetic and structural  
41  
42 signature for PPAR $\gamma$  partial agonism. *ACS Chem. Biol.* **2016**, *11*, 273-283.
- 43  
44 (4) Taygerly, J. P.; McGee, L. R.; Rubenstein, S. M.; Houze, J. B.; Cushing, T. D.; Li, Y.;  
45  
46 Motani, A.; Chen, J. L.; Frankmoelle, W.; Ye, G.; Learned, M. R.; Jaen, J.; Miao, S.; Timmermans, P.  
47  
48 B.; Thoolen, M.; Kearney, P.; Flygare, J.; Beckmann, H.; Weiszmann, J.; Lindstrom, M.; Walker, N.;  
49  
50 Liu, J.; Biermann, D.; Wang, Z.; Hagiwara, A.; Iida, T.; Aramaki, H.; Kitao, Y.; Shinkai, H.;  
51  
52 Furukawa, N.; Nishiu, J.; Nakamura, M. Discovery of INT131: a selective PPAR $\gamma$  modulator  
53  
54 that enhances insulin sensitivity. *Bioorg. Med. Chem.* **2013**, *21*, 979-992.  
55  
56  
57  
58  
59  
60

- 1  
2  
3 (5) Barroso, I.; Gurnell, M.; Crowley, V. E.; Agostini, M.; Schwabe, J. W.; Soos, M. A.; Maslen,  
4 G. L.; Williams, T. D.; Lewis, H.; Schafer, A. J.; Chatterjee, V. K.; O'Rahilly, S. Dominant negative  
5 mutations in human PPARgamma associated with severe insulin resistance, diabetes mellitus and  
6 hypertension. *Nature* **1999**, *402*, 880-883.  
7  
8  
9  
10  
11 (6) Choi, J. H.; Banks, A. S.; Estall, J. L.; Kajimura, S.; Bostrom, P.; Laznik, D.; Ruas, J. L.;  
12 Chalmers, M. J.; Kamenecka, T. M.; Bluher, M.; Griffin, P. R.; Spiegelman, B. M. Anti-diabetic  
13 drugs inhibit obesity-linked phosphorylation of PPARgamma by Cdk5. *Nature* **2010**, *466*, 451-456.  
14  
15  
16  
17 (7) Choi, J. H.; Banks, A. S.; Kamenecka, T. M.; Busby, S. A.; Chalmers, M. J.; Kumar, N.;  
18 Kuruvilla, D. S.; Shin, Y.; He, Y.; Bruning, J. B.; Marciano, D. P.; Cameron, M. D.; Laznik, D.;  
19 Jurczak, M. J.; Schurer, S. C.; Vidovic, D.; Shulman, G. I.; Spiegelman, B. M.; Griffin, P. R.  
20 Antidiabetic actions of a non-agonist PPARgamma ligand blocking Cdk5-mediated phosphorylation.  
21 *Nature* **2011**, *477*, 477-481.  
22  
23  
24  
25  
26  
27 (8) Wakabayashi, K.; Hayashi, S.; Matsui, Y.; Matsumoto, T.; Furukawa, A.; Kuroha, M.;  
28 Tanaka, N.; Inaba, T.; Kanda, S.; Tanaka, J.; Okuyama, R.; Wakimoto, S.; Ogata, T.; Araki, K.;  
29 Ohsumi, J. Pharmacology and in vitro profiling of a novel peroxisome proliferator-activated receptor  
30 gamma ligand, Cerco-A. *Biol. Pharm. Bull.* **2011**, *34*, 1094-1104.  
31  
32  
33  
34  
35  
36 (9) Berger, J. P.; Petro, A. E.; Macnaul, K. L.; Kelly, L. J.; Zhang, B. B.; Richards, K.; Elbrecht,  
37 A.; Johnson, B. A.; Zhou, G.; Doebber, T. W.; Biswas, C.; Parikh, M.; Sharma, N.; Tanen, M. R.;  
38 Thompson, G. M.; Ventre, J.; Adams, A. D.; Mosley, R.; Surwit, R. S.; Moller, D. E. Distinct  
39 properties and advantages of a novel peroxisome proliferator-activated protein [gamma] selective  
40 modulator. *Mol. Endocrinol.* **2003**, *17*, 662-676.  
41  
42  
43  
44  
45  
46 (10) DePaoli, A. M.; Higgins, L. S.; Henry, R. R.; Mantzoros, C.; Dunn, F. L. Can a selective  
47 PPARgamma modulator improve glycemic control in patients with type 2 diabetes with fewer side  
48 effects compared with pioglitazone? *Diabetes Care* **2014**, *37*, 1918-1923.  
49  
50  
51  
52 (11) Motani, A.; Wang, Z.; Weiszmann, J.; McGee, L. R.; Lee, G.; Liu, Q.; Staunton, J.; Fang, Z.;  
53 Fuentes, H.; Lindstrom, M.; Liu, J.; Biermann, D. H.; Jaen, J.; Walker, N. P.; Learned, R. M.; Chen, J.  
54 L.; Li, Y. INT131: a selective modulator of PPAR gamma. *J. Mol. Biol.* **2009**, *386*, 1301-1311.  
55  
56  
57  
58  
59  
60

- 1  
2  
3 (12) Higgins, L. S.; Mantzoros, C. S. The development of INT131 as a selective PPARgamma  
4 modulator: approach to a safer insulin sensitizer. *PPAR Res.* **2008**, *2008*, 936906.  
5  
6  
7 (13) McGee, L. R.; Rubenstein, S. M.; Houze, J. B. Discovery of AMG131: a selective modulator  
8 of PPAR $\gamma$ . *Proceedings of the 231st American Chemical Society National Meeting* **2006**.  
9  
10  
11 (14) Banks, A. S.; McAllister, F. E.; Camporez, J. P.; Zushin, P. J.; Jurczak, M. J.; Laznik-  
12 Bogoslavski, D.; Shulman, G. I.; Gygi, S. P.; Spiegelman, B. M. An ERK/Cdk5 axis controls the  
13 diabetogenic actions of PPARgamma. *Nature* **2015**, *517*, 391-395.  
14  
15  
16  
17 (15) Puhl, A. C.; Bernardes, A.; Silveira, R. L.; Yuan, J.; Campos, J. L.; Saidemberg, D. M.;  
18 Palma, M. S.; Cvorovic, A.; Ayers, S. D.; Webb, P.; Reinach, P. S.; Skaf, M. S.; Polikarpov, I. Mode of  
19 peroxisome proliferator-activated receptor gamma activation by luteolin. *Mol. Pharmacol.* **2012**, *81*,  
20 788-799.  
21  
22  
23  
24  
25 (16) Tontonoz, P.; Spiegelman, B. M. Fat and beyond: the diverse biology of PPARgamma. *Annu.*  
26 *Rev. Biochem.* **2008**, *77*, 289-312.  
27  
28  
29 (17) Nolte, R. T.; Wisely, G. B.; Westin, S.; Cobb, J. E.; Lambert, M. H.; Kurokawa, R.;  
30 Rosenfeld, M. G.; Willson, T. M.; Glass, C. K.; Milburn, M. V. Ligand binding and co-activator  
31 assembly of the peroxisome proliferator-activated receptor-gamma. *Nature* **1998**, *395*, 137-143.  
32  
33  
34  
35 (18) Wheeler, S. E. Understanding substituent effects in noncovalent interactions involving  
36 aromatic rings. *Acc. Chem. Res.* **2013**, *46*, 1029-1038.  
37  
38  
39 (19) Powell, H. R.; Johnson, O.; Leslie, A. G. Autoindexing diffraction images with iMosflm.  
40 *Acta. Crystallogr. D Biol. Crystallogr.* **2013**, *69*, 1195-203.  
41  
42  
43 (20) Evans, P. R.; Murshudov, G. N. How good are my data and what is the resolution? *Acta.*  
44 *Crystallogr. D Biol. Crystallogr.* **2013**, *69*, 1204-1214.  
45  
46  
47 (21) Karplus, P. A.; Diederichs, K. Linking crystallographic model and data quality. *Science* **2012**,  
48 336, 1030-1033.  
49  
50  
51 (22) McCoy, A. J.; Grosse-Kunstleve, R. W.; Adams, P. D.; Winn, M. D.; Storoni, L. C.; Read, R.  
52 J. Phaser crystallographic software. *J. Appl. Crystallogr.* **2007**, *40*, 658-674.  
53  
54  
55 (23) Zwart, P. H.; Afonine, P. V.; Grosse-Kunstleve, R. W.; Hung, L. W.; Ioerger, T. R.; McCoy,  
56 A. J.; McKee, E.; Moriarty, N. W.; Read, R. J.; Sacchettini, J. C.; Sauter, N. K.; Storoni, L. C.;  
57  
58  
59  
60

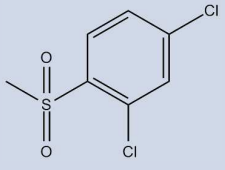
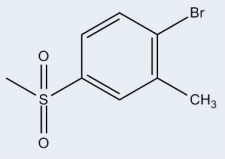
Terwilliger, T. C.; Adams, P. D. Automated structure solution with the PHENIX suite. *Methods Mol. Biol.* **2008**, *426*, 419-435.

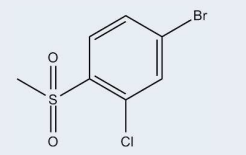
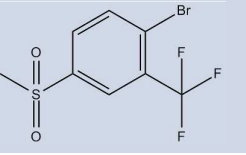
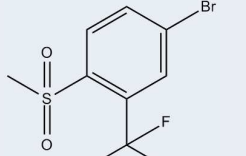
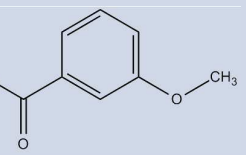
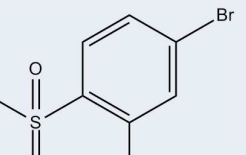
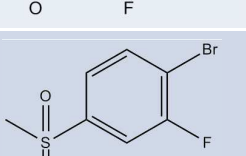
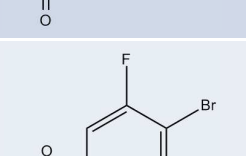
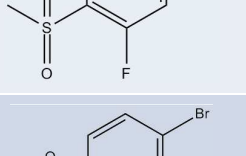
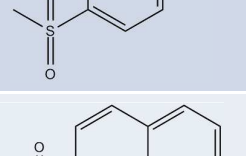
(24) Emsley, P.; Cowtan, K. Coot: model-building tools for molecular graphics. *Acta Crystallogr. D Biol. Crystallogr.* **2004**, *60*, 2126-2132.

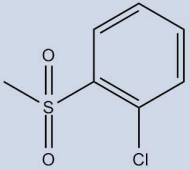
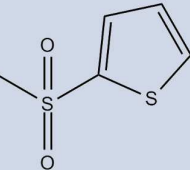
(25) McPhillips, T. M.; McPhillips, S. E.; Chiu, H. J.; Cohen, A. E.; Deacon, A. M.; Ellis, P. J.; Garman, E.; Gonzalez, A.; Sauter, N. K.; Phizackerley, R. P.; Soltis, S. M.; Kuhn, P. Blu-Ice and the distributed control system: software for data acquisition and instrument control at macromolecular crystallography beamlines. *J. Synchrotron Radiat.* **2002**, *9*, 401-406.

(26) Abagyan, R.; Totrov, M. Biased probability Monte Carlo conformational searches and electrostatic calculations for peptides and proteins. *J. Mol. Biol.* **1994**, *235*, 983-1002.

**Table 1. Structure Activity of Compound 1 Analogs.** Each data point in the EC<sub>50</sub> does response was repeated in triplicate and standard deviation was derived from these values. In addition, two biological replicates were performed to ensure reproducibility of the data.

Formula	Compound	EC <sub>50</sub> (nM) n=3	Trans-activation (%)* n=2	Percent Purity (%)
	<b>1 (INT131)</b>	170±10	24±4	>95
	<b>2</b>	600±61	29±6	>99
	<b>3</b>	4±1	21±9	>99

	<b>4</b>	134±13	27±8	85
	<b>5</b>	957±499	18±7	97
	<b>6</b>	94±10	34±10	93
	<b>7</b>	ND	2±1	>99
	<b>8</b>	2±1	13±7	88
	<b>9</b>	169±14	9±5	94
	<b>10</b>	131±6	10±6	> 98
	<b>11</b>	151±20	11±6	96
	<b>12</b>	4289±289	23±12	90

	<b>13</b>	5810±945	19±11	99
	<b>14</b>	3314±2923	14±6	>99
	<b>15</b>	ND	14±8	>99

**Table 2.** Crystallographic Data.

Parameter	Compound (10)
Space group	C2
Cell dimensions <i>a</i> , <i>b</i> , <i>c</i> (Å)	93.1, 62.2, 118.9
Monoclinic angle β (deg)	102.2
X-ray source	Synchrotron: APS 22-ID
Wavelength (Å)	1.0
Resolution range (Å)	50-2.24
Last shell (Å)	2.32-2.25
R <sub>merge</sub> (%)	0.051 (0.178)

Observations	146759 (13592)
Unique reflections	31321 (2946)
Mean (I)/ $\sigma$ (I)	15.3 (5.9)
Completeness	98.0 (99.7)
Multiplicity	4.7 (4.6)
Structure refinement	
Resolution range (Å)	45.5-2.24
R <sub>work</sub> (%)	0.2039
R <sub>free</sub> (%)	0.2555
Total number of	
Non-hydrogen atoms	
Protein atoms	4139
Ligand atoms	64
Water molecules	159
RMSD	
Bond length (Å)	0.007
Bond angle (deg)	0.878
B-factors (Å <sup>2</sup> )	
Overall	61.2

Average protein atoms	61.3
Average ligand atoms	63.2
Average solvent	58.8
Ramachandran statistics	
Most favoured regions (%)	96.5
Allowed regions (%)	3.29
Disallowed regions (%)	0.19

<sup>a</sup>Values in parentheses are for the highest resolution shell.

## FIGURE LEGENDS

**Figure 1: Chemical composition of partial agonist 1.** The compound is comprised of three major moieties, denoted A, B, and C. The potential substitution positions on ring A are numbered.

**Figure 2: Crystal structure of 10 bound to PPAR $\gamma$  LBD.** (A) Ribbons diagram of the PPAR $\gamma$  LBD (green) in complex with 10 (blue sticks). (B) Comparison of 10 (blue sticks) binding mode to 1 (yellow sticks), with the main scaffold in the same position and some similar hydrogen bonds formed (1 PDB:3FUR)<sup>11</sup>. (C) Superimposition of 10 and 1 (PDB:3FUR) in the region contacting the beta-sheet and H3.

1  
2  
3 **Figure 3: Superimposition of docked 0 analogs.** The ligands (colored sticks) that have been  
4 shown to bind to PPAR $\gamma$  were docked *in silico* to the PPAR $\gamma$  LBD receptor (blue ribbons).  
5 The scaffold of the ligands binds in a similar position, with slight variations at ring A due to  
6 substitutions at that location.  
7  
8  
9

10  
11  
12 **Figure 4: The substitution of a sulfonamide for an amide linker has detrimental effects**  
13 **on the capability of 7 to bind to PPAR $\gamma$ .** Shown is a superimposition of the 7 structure  
14 (white) with the 1 structure (green). The carbon of the C=O in 7 (white sticks) is confined to a  
15 planar conformation which prevents the A ring of 7 from making favorable *pi-pi* interactions  
16 with Phe363 as well as hydrophobic interactions with residues of the binding pocket.  
17  
18  
19  
20  
21  
22  
23

24  
25 **Figure 5: Superimposition of ligands containing a 4-Br substitution in benzene ring A**  
26 **reveal very similar positions of the bromine atom within the binding pocket.** Shown is a  
27 superimposition of the compounds containing a bromine atom at position 4 (colored sticks)  
28 bound to PPAR $\gamma$  (green ribbons). A bromine at position 4 of ring A results in higher affinity  
29 of the ligand. The presence of a Br atom in this position enables a weak hydrogen bond with  
30 the backbone nitrogen of Phe282 (shown as dashes).  
31  
32  
33  
34  
35  
36  
37  
38

39 **Figure 6: Effective space filling within the PPAR $\gamma$  LBD binding pocket has been shown**  
40 **to correlate with higher affinities.** Displayed are superimpositions of the compound 1  
41 analogs (colored sticks) bound to PPAR $\gamma$  (ribbons, green or blue), and a surface  
42 representation of the ligand binding pocket (grey surface). Ligands with substitutions at (A)  
43 position 2 of ring A have better packing within the pocket and higher affinities than (B) those  
44 which have substitutions at other positions. Ligands with substitutions at position 2 include 3  
45 (red), 4 (orange), 6 (green), and 8 (cyan). Ligands with additional substitutions at positions 3  
46 or 5 have lower affinities and include 2 (yellow), 5 (pale orange), 9 (teal), 11 (purple), 2-  
47 chloro-N-(3,5-dichloro-4-(quinolin-3-yloxy)phenyl)benzenesulfonamide (13) (light blue), 14  
48  
49  
50  
51  
52  
53  
54  
55  
56  
57  
58  
59  
60

1  
2  
3 (turquoise) **15** (lilac), and **10** (dark blue). (C) The oxygen linker in the trifluoro substitution of  
4  
5 **3** enables it to reach further into the binding pocket than **6** and confer a better lock-and-key fit  
6  
7 in addition to forming additional hydrogen bonds with Gln286. (D) the naphthalene moiety of  
8  
9 **12** (pink) extends as far into the binding pocket as other ligands, as shown by comparison  
10  
11 with **9** (teal), **10** (dark blue), and **11** (purple).

12  
13  
14  
15 **Figure 7: The naphthalene substitution at position A of 12 enables extensive**  
16  
17 **hydrophobic contacts contributed by helices 3 and 7.** Shown is a superimposition of the **1**  
18  
19 (yellow sticks) and **12** (purple sticks) compounds bound to the PPAR $\gamma$  LBD (green ribbons).  
20  
21 The naphthalene moiety of **12** (purple) is more hydrophobic than other ligands, enabling  
22  
23 unique hydrophobic interactions with the PPAR $\gamma$  binding pocket. Structure compared to **1**  
24  
25 (yellow).

26  
27  
28  
29  
30  
31  
32  
33  
34  
35  
36  
37  
38  
39  
40 **Table of Contents Graphic**

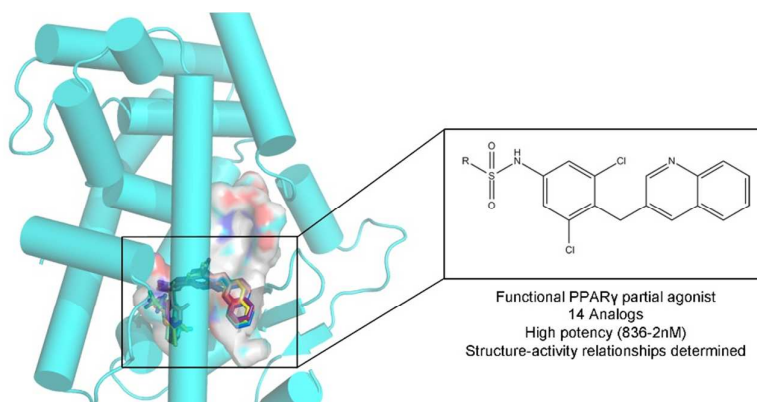


Figure 1

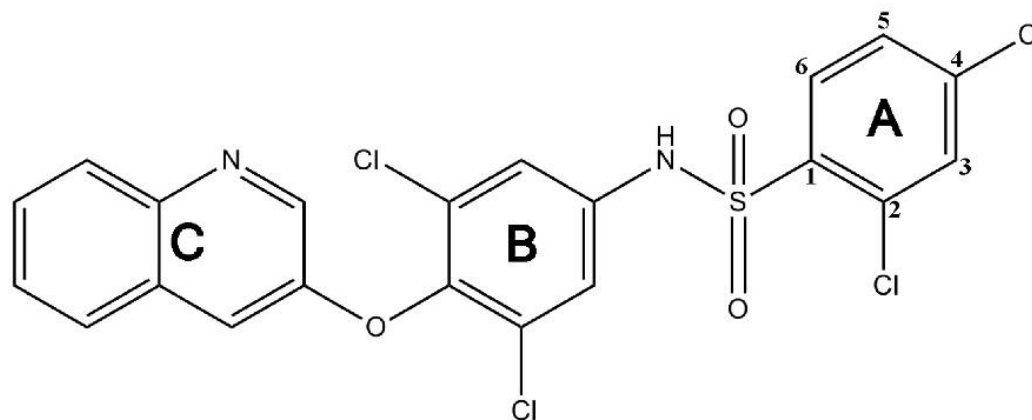


Figure 2

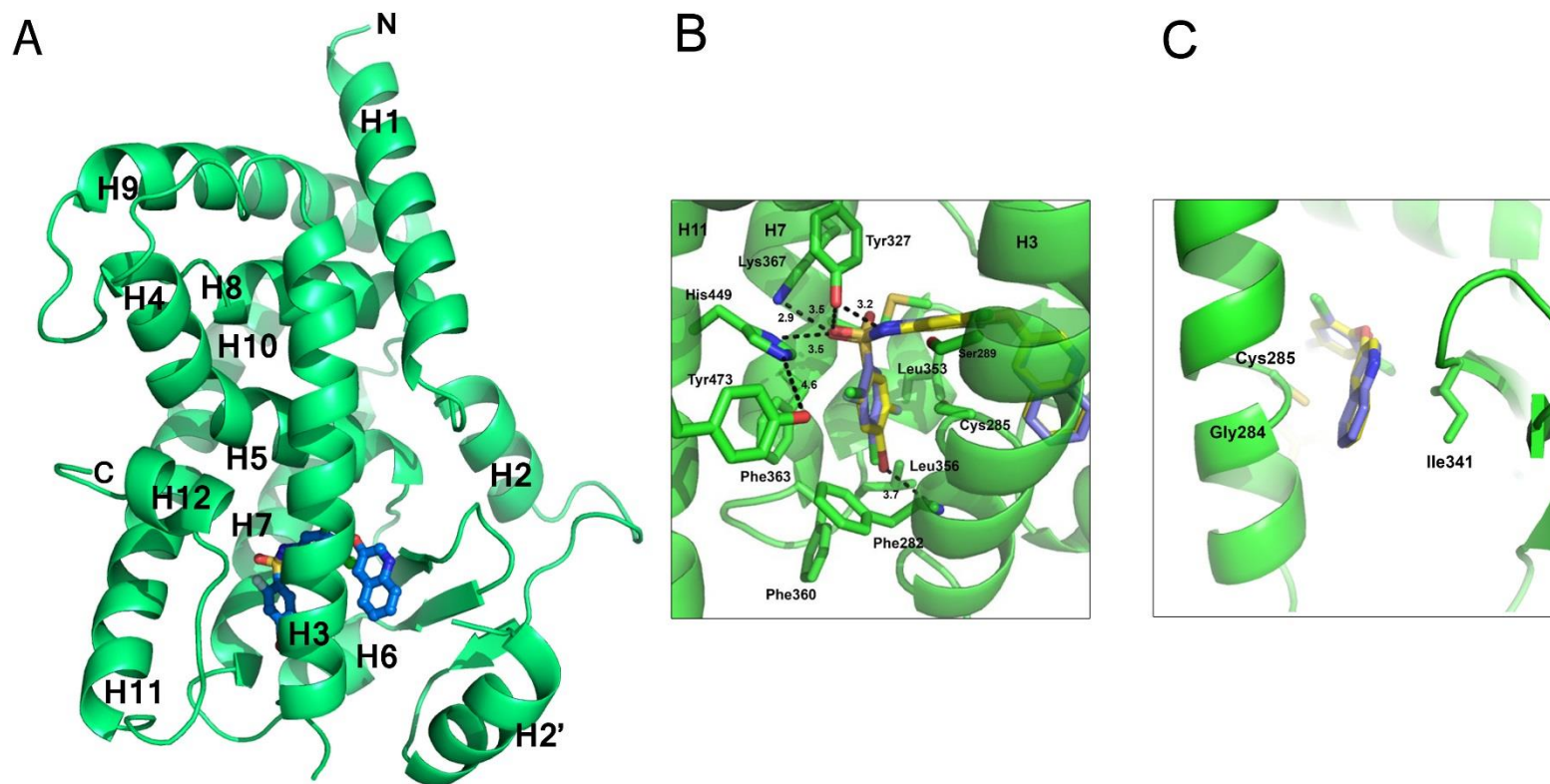
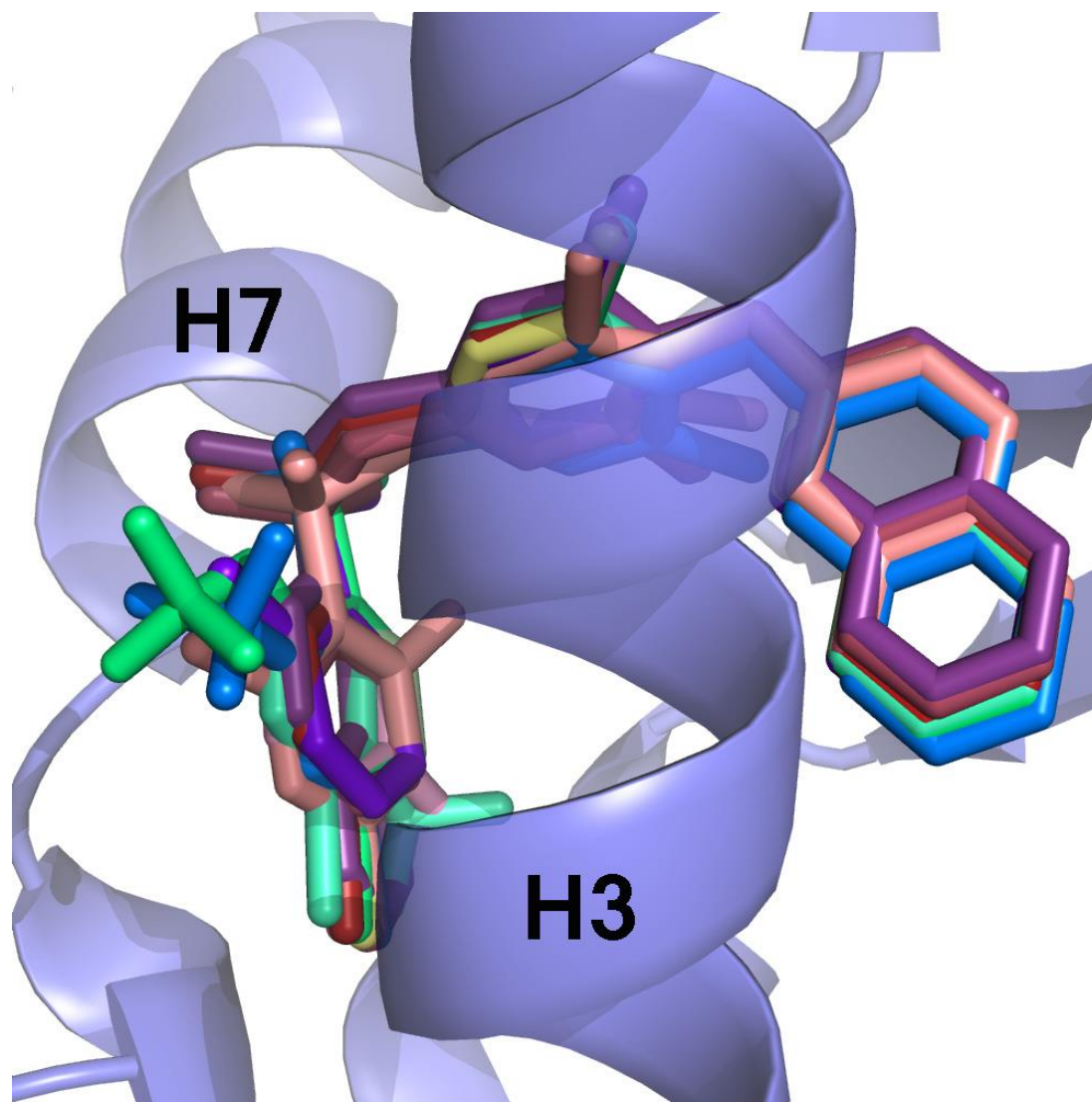


Figure 3



ACS Paragon Plus Environment

Figure 4

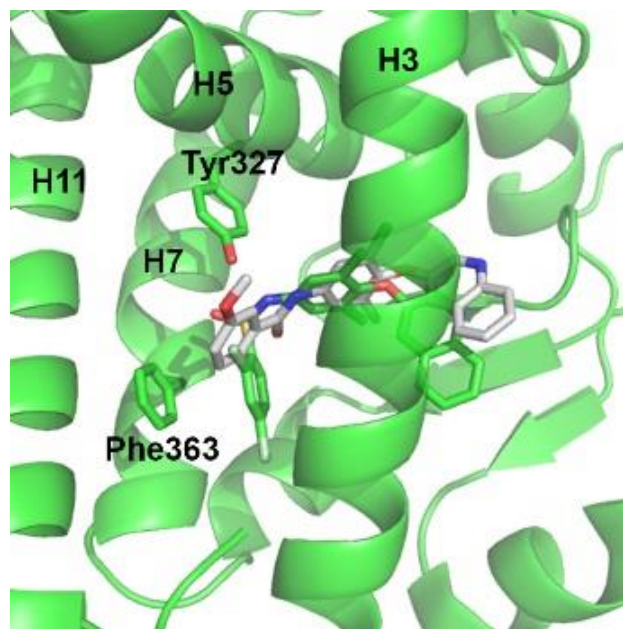


Figure 5

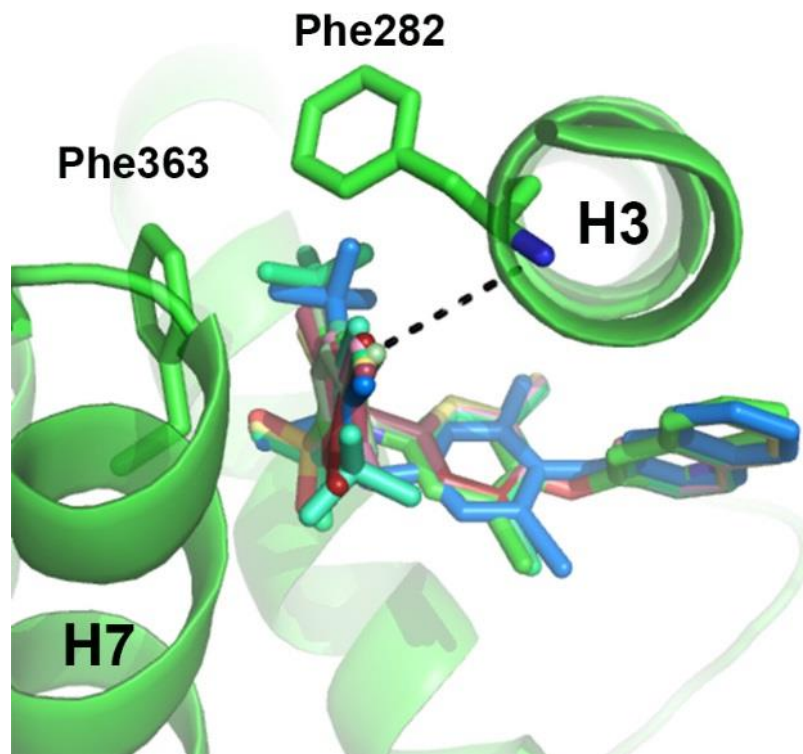


Figure 6

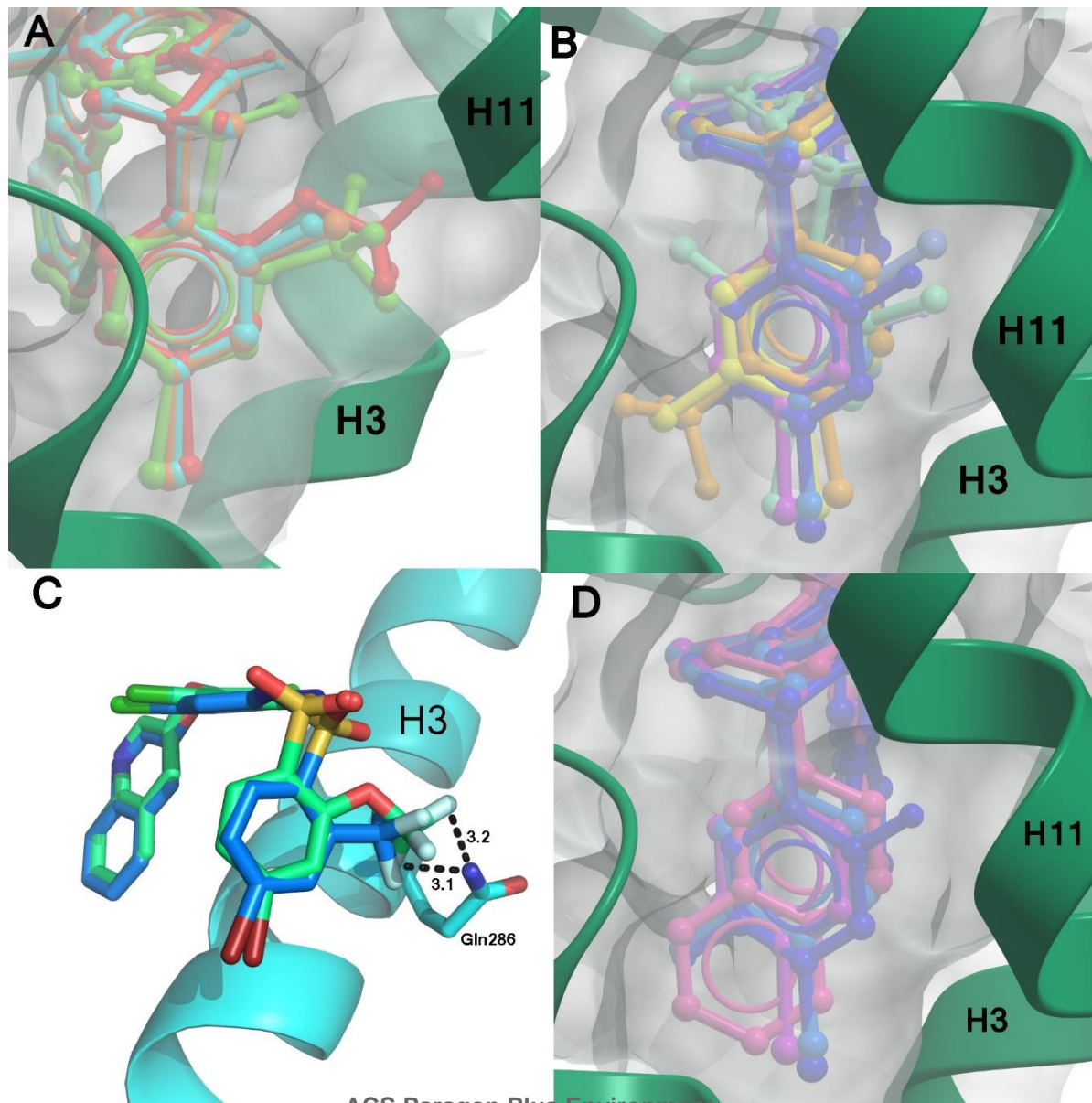


Figure 7

